Revista Facultad de Ingeniería Universidad de Antioquia
ISSN: 0120-6230
ISSN: 2422-2844
Facultad de Ingeniería, Universidad de Antioquia

Arbeláez Pérez, Oscar Felipe; Domínguez Cardozo, Sara; Orrego Romero, Andrés Felipe; Villa Holguín, Aída Luz; Bustamante, Felipe

Gas phase synthesis of dimethyl carbonate from CO2 and CH3OH over Cu-Ni/AC. A kinetic study

Revista Facultad de Ingeniería Universidad de Antioquia, no. 95, 2020, April-June, pp. 88-99
Facultad de Ingeniería, Universidad de Antioquia

DOI: 10.17533/udea.redin.20190941

Available in: http://www.redalyc.org/articulo.oa?id=43063710009

redin Revista Facultad de Ingeniería, Universidad de Antioquia, No.95, pp. 88-99, Apr-Jun 2020

Gas phase synthesis of dimethyl carbonate from CO_2 and CH_3OH over Cu-Ni/AC. A kinetic study

Síntesis en fase gaseosa de dimetil carbonato con CO_2 y CH_3OH sobre Cu-Ni/AC. Estudio cinético

Oscar Felipe Arbeláez Pérez [1*], **Sara Domínguez Cardozo** [2], **Andrés Felipe Orrego Romero** [2], **Aída Luz Villa Holguín** [2], **Felipe Bustamante** [2]

[1]TERMOMEC, Facultad de Ingeniería, Universidad Cooperativa de Colombia. Calle 50 # 41-74. C. P. 050016. Medellín, Colombia.
[2]Environmental Catalysis Research Group, Departamento de Ingeniería Química, Facultad de Ingeniería, Universidad de Antioquia UdeA. Calle 70 # 52-21. C. P. 050010. Medellín, Colombia.

CITE THIS ARTICLE AS:

O. F. Arbelaez, S. Domínguez, A. F Orrego, A. L. Villa and F. Bustamante. "Gas phase synthesis of dimethyl carbonate from CO_2 and CH_3OH over Cu-Ni/AC. A kinetic study", *Revista Facultad de Ingeniería Universidad de Antioquia*, no. 95, pp. 88-99, Apr-Jun 2020. [Online]. Available: https://www.doi.org/10.17533/udea.redin.20190941

ARTICLE INFO:

Received: May 09, 2019
Accepted: September 20, 2019
Available online: September 23, 2019

KEYWORDS:

Methanol; catalysts; reaction mechanism; reaction rate; *in situ* FT-IR analysis

Metanol; catalizadores; mecanismo de reacción; velocidad de reacción; análisis FT-IR *in situ*

ABSTRACT: The catalytic activity for dimethyl carbonate formation from carbon dioxide and methanol over mono and bimetallic Cu:Ni supported on activated carbon is presented. Bimetallic catalysts exhibit higher catalytic activity than the monometallic samples, being Cu:Ni-2:1 (molar ratio) the best catalyst; X-Ray diffraction, transmission electron microscopy, and metal dispersion analysis provided insight into the improved activity. *In situ* FT-IR experiments were conducted to investigate the mechanism of formation of dimethyl carbonate from methanol and carbon dioxide over Cu-Ni:2-1. The kinetics of the direct synthesis of dimethyl carbonate in gas phase over Cu:Ni-2:1 supported on activated carbon catalyst was experimentally investigated at 12 bar and temperatures between 90 °C and 130 °C, varying the partial pressures of CO_2 and methanol. Experimental kinetic data were consistent with a Langmuir–Hinshelwood model that included carbon dioxide and methanol adsorption on catalyst actives sites (Cu, Ni and Cu-Ni), and the reaction of adsorbed CO_2 with methoxi species as the rate determining step. The estimated apparent activation energy was 94.2 kJ mol^{-1}.

RESUMEN: Se reporta la actividad catalítica en la formación de dimetil carbonato a partir de dióxido de carbono y metanol sobre catalizadores mono y bimetálicos de Cu-Ni soportado en carbón activado. Los catalizadores bimetálicos presentaron una mayor actividad catalítica que los monometálicos, siendo la muestra Cu:Ni-2:1 el mejor catalizador. La caracterización de los materiales mediante análisis de difracción de rayos X, microscopía electrónica de transmisión y dispersión metálica permitieron sugerir una explicación al porqué de su mejor desempeño. Se realizaron experimentos de FT-IR *in situ* para investigar el mecanismo de formación de carbonato de dimetilo a partir de metanol y dióxido de carbono sobre Cu-Ni:2-1. Se estudió la cinética de la síntesis directa de dimetil carbonato en fase gaseosa sobre Cu:Ni-2:1 soportado en carbón activado, a 12 bar y temperaturas entre 90 °C y 130 °C, como función de la presión parcial del dióxido de carbono y del metanol. Los datos experimentales fueron consistentes con un mecanismo Langmuir-Hinshelwood, el cual incluyó la adsorción de dióxido de carbono y metanol sobre los sitios activos del catalizador (Cu, Ni, y Cu-Ni), siendo la reacción del dióxido de carbono adsorbido con las especies metoxi como etapa limitante. La energía de activación aparente estimada de la reacción fue 94,2 kJ mol^{-1}.

1. Introduction

Dimethyl carbonate (DMC) has a wide range of applications, such as organic solvent [1], raw material in the production of polyurethanes and polycarbonates [2], methylating [3] and carbonylating agent [4], electrolyte solvent in lithium batteries [5], and fuel additive [6].

* Corresponding author: Oscar Felipe Arbeláez Pérez
E-mail: oscar.arbelaez@campusucc.edu.co
ISSN 0120-6230
e-ISSN 2422-2844

DOI: 10.17533/udea.redin.20190941

DMC is produced by several catalytic routes including phosgenation of methanol [7], transesterification of urea and methanol [8], oxidative carbonylation of methanol [9], transesterification of ethyl carbonate and methanol [10], carbonylation of methyl nitrite [11], and methanolysis of carbon dioxide. The direct synthesis of DMC from CO_2 and methanol is a green chemical route that would replace toxic and corrosive reagents, such as phosgene, ammonia, carbon monoxide, hydrogen chloride or dimethyl sulphate, by low-cost carbon dioxide. However, the direct synthesis of DMC is thermodynamically limited and low yields are obtained, which can be overcome, respectively, with the efficient removal of water from the reaction mixture (e.g., by using hydrophilic membranes or water traps), and the design of novel catalysts. Catalytic synthesis of dimethyl carbonate from methanol and carbon dioxide have been carried out over K_2CO_3 [12], CH_3OK [13], ZrO_2 [14] ZrO_2-CeO_2 [15], CeO_2 [16], Al_2O_3-CeO_2 [17], and $Ga_2O_3/Ce_xZr_{1-x}O_2$ [18] catalysts. The batch reaction is conducted at high pressure (4 MPa) in almost all cases, however, increasing operational costs. A gas-phase process, on the other hand, would facilitate process control and catalyst recovery, reducing operational and capital costs and smoothing the scaling-up of a continuous process. Table 1 shows the activity and reaction conditions reported for gas phase synthesis of DMC with heterogeneous catalysts.

According to Table 1, reported methanol conversion is above 0.58%, which, albeit low, is close to the expected equilibrium value [28]; additionally, catalysts exhibited high selectivity to the desired product. Furthermore, Cu-Ni bimetallic catalysts present higher catalytic activity than the Cu and Ni monometallic samples, possibly due to the synergetic effect of Cu, Ni and Cu–Ni alloy (evidenced by XRD [23]) in the activation of reactants. It can also be observed that the kind of support plays an important role in the activity, being supports based on carbonaceous materials the ones that most favor activity (see Table 1, entries 6, 9, 10, 13). Therefore, selecting a suitable supporting material is a crucial factor to get highly effective catalysts. In particular, activated carbon, an inexpensive and available material, displays high surface area and high mechanical, chemical and thermal stability.

In order to scale the gas-phase reaction, information on the kinetics of DMC synthesis in gas phase is required. Kinetic studies of the liquid phase synthesis of DMC from methanol and carbon dioxide over CeO_2 [29] and CeO_2 nanorod catalysts [30] have been reported. A reaction rate based on the Langmuir-Hinshelwood mechanism was proposed, including the following steps: adsorption of methanol and carbon dioxide over CeO_2 sites, reaction between adsorbed species ($MeOH^* + CO_2^*$) and desorption of the products (DMC and H_2O); the surface reaction is the limiting step [29], [30]. The activation energy of the reaction reported was 106 kJ mol^{-1} [29] and 65 kJ mol^{-1} [30]. However, kinetic results, which are essential to develop a kinetic model that would allow evaluating novel integrated processes to overcome the low equilibrium conversion, are very scarce. In this contribution, the kinetic study of dimethyl carbonate gas phase synthesis over Cu:Ni-2:1 supported on activated carbon is presented. Catalytic activity and characterization of the bimetallic and monometallic samples is also discussed. *In-situ* FTIR helped elucidate the nature of the adsorbed species formed during the dimethyl carbonate synthesis and validated the proposed kinetic model.

2. Experimental section

2.1 Catalyst synthesis

In order to remove mineral impurities and improve its hydrophilicity, the activated carbon (AC) (Merck) was treated with 2 M HCl solution for 12 h in boiling water under reflux, followed by filtering and washing with deionized water, and drying at 100 °C for 12 h. The AC was further oxidized with 4 M H_2SO_4, filtered and washed until neutral pH, and dried in air (110 °C, 24 h). AC was stored in desiccators before using them as catalyst supports. Mono and bimetallic catalysts were prepared by conventional wetness impregnation on the treated AC, previously reported [31], using $Cu(NO_3)_2{\cdot}3H_2O$ (Carlo Erba, 99.5%) and $Ni(NO_3)_2{\cdot}6H_2O$ (Merck, 99%) dissolved in ammonia solution. Different Cu:Ni molar ratio (3:1, 2:1, 1:1, 1:2, 1:3) were prepared, with a nominal metal oxide loading (CuO + NiO) of 15 wt.%. After addition of the precursor solutions to the activated carbon, the resulting mixtures were stirred at room temperature for 24 h, and then dried at 90 °C during 12 h. After drying, the solids were calcined in a N_2 stream (25 mL min^{-1}) at 500 °C for 2 h (heating ramp 0.5 °C min^{-1}) and then reduced in a 5% H_2/Ar stream at 600 °C for 3 h (heating ramp 0.5 °C min^{-1}).

2.2 Catalyst characterization

X-Ray diffraction (XRD)

The crystallinity of the synthesized materials was determined at room temperature by X-ray diffraction (XRD) of the reduced catalyst on a Phillips PW 1740 diffractometer using Cu Kα radiation and Ni filter operated at 40 kV and 20 mA. The 2θ scanning range was 5 - 70° at 2° min^{-1}. The diffractograms were compared to JCPDS (Joint Committee of Powder Diffraction Standards) data. The crystallite size of mono and bimetallic particles was calculated from the broadening of X-ray diffraction

Table 1 Heterogeneous catalysts reported for gas-phase synthesis of DMC

Entry	Catalyst	T(°C), P (bar)	CH_3OH conversion (%)	DMC selectivity (%)	Author, year [Reference]
1	Ni–Cu/MoSiO	140, 1	16.4	86.5	Zhong, 2000 [19]
2	Ni–Cu/VSiO	140, 1	14.5	87.8	Zhong, 2000 [19]
3	Cu-KF/MgSiO	130, 10	5.31	88.9	Li, 2003 [20]
4	Cu/GO*	110, 12	2.51	92.3	Bian, 2009 [21]
5	Ni/GO*	110, 12	0.79	91.1	Bian, 2009 [21]
6	Cu-Ni/GO*	110, 12	7.78	88.5	Bian, 2009 [21]
7	Cu/AC*	110, 12	2.16	92.5	Bian, 2009 [21]
8	Ni/AC*	110, 12	1.43	91.6	Bian, 2009 [21]
9	Cu-Ni/AC*	110, 12	6.44	88.9	Bian, 2009 [21]
10	Cu-Ni/MWCNTs*	120, 12	4.36	85.8	Bian, 2009 [22]
11	Cu/graphite*	100, 12	2.51	92.3	Bian, 2009 [23]
12	Ni/graphite*	100, 12	0.79	91.1	Bian, 2009 [23]
13	Cu-Ni/graphite*	100, 12	10.13	90.2	Bian, 2009 [23]
14	$Co_{1.5}PW_{12}O_{40}$	200, 1	7.60	86.5	Aouissi, 2010 [24]
15	$CuCl_2$/AC**	120, 12	r_{DMC} = 4.77***	90.1	Bian, 2010 [25]
16	Cu/diatomite*	120,12	2.31	92.0	Chen, 2012 [26]
17	Ni/diatomite*	120,12	0.58	91.5	Chen, 2012 [26]
18	Cu–Ni/diatomite*	120, 12	4.05	88.7	Chen, 2012 [26]
19	Cu–Ni/MS*	120, 11	7.1	87.0	Chen, 2012 [27]

GO: graphite oxide, AC: activated carbon, MWCNTs: multi-walled carbon nanotubes, MS: molecular sieve,* Cu/Ni molar ratio 2/1, metal loading (CuO + NiO) = 20%. ** Cu loading 7%, *** rDMC formation rate [mmol h^{-1}].

pattern using the Scherrer's equation, Equation 1

$$D = \frac{K\lambda}{(\beta_m - \beta_i)\cos\theta} \quad (1)$$

Where, D is the average crystallite size (nm); K is the Scherrer's constant (K= 0.94 for spherical crystals with cubic symmetry); λ is the radiation wavelength (0.154 nm); ($\beta_m\beta_i$) is the broadening of the full width at half maximum of the main peak, β_m: sample; β_i: reference = 0.11; and, θ is the Bragg's angle (degrees).

Surface area

Nitrogen adsorption/desorption isotherms of catalysts were determined by N2 physisorption of liquid nitrogen at -196 °C, using a Micromeritics 2375 BET instrument equipped with a Vacprep 061 degasser. Prior to the experiments, samples were degassed for 2 h at 250 °C and 1.5×10^{-4} bar to ensure a clean and dry surface. The Brunauer-Emmett-Teller (BET) and the Barrett-Joyner-Halenda (BHJ) approaches were used to determine the surface area and the pore size distribution of the samples, respectively.

CO pulse chemisorption

CO pulse chemisorption experiments were carried out in a Micromeritics Autochem II 2920 device. Prior to the analysis, 50 mg samples were pre-reduced in flowing 5% H_2/Ar mixture (50 mL min^{-1}) at 120°C and 220°C during 30 min at each temperature, and at 350°C for 2 h; heating rate was 10°C min^{-1} between steps. Then, samples were purged in helium at 350°C for 1.5 h and cooled to 35°C in flowing He. Pulses of a 1% CO/He mixture (0.8318 mL) were injected at 35°C into the chamber holding the sample; injection was repeated 20 times at 4 min intervals. Metal dispersion (see Equation 2) was determined by assuming the adsorption stoichiometry of one carbon monoxide molecule per nickel or copper surface atom (CO/Ni = CO/Cu 1).

$$\text{Metal dispersion} = \frac{\text{consumed CO} \times M \times MW \times F}{\text{Mxbulk}} \times 100 \quad (2)$$

Consumed CO = quantity of consumed or chemisorbed CO [mol g^{-1}]; M = mass of the catalyst [g]; MW = molecular weight of metal (Cu or Ni) [g mol^{-1}]; F = stoichiometric factor (CO:Cu 1:1 and CO:Ni 1:1); and, $Mxbulk$ = mass metal (Cu or Ni). In bimetallic catalysts dispersion was calculated as the sum of Cu and Ni dispersion.

Transmission Electron Microscopy (TEM)

The particle morphology, size and size distribution of metal particles dispersed on the catalyst were characterized by TEM (JEOL JEM-2100F/UHR). The system was operated with an accelerating voltage of 200 kV and emission current of 124 μA. Several TEM micrographs were recorded and analyzed for particle size distribution. At least 100 metal

nanoparticles per sample were analyzed to determine the average size and size distribution.

Temperature Programmed Reduction (TPR)

H_2-TPR experiments of calcined catalyst samples were performed in a Micromeritics AutoChem II 2920 apparatus. Samples (50 mg) were pretreated at 5°C min^{-1} to 250 °C for 1 h in flowing helium (70 mL min^{-1}), and then cooled to 40 °C. Thereafter, the samples were heated to 800 °C using 5% H_2/Ar (70 mL min^{-1}) at 8 °C min^{-1}. The signals of H_2 consumption were continuously monitored by a thermal conductivity detector (TCD). The reducibility of the samples (%) was calculated as the ratio of the theoretical and experimental H_2 consumption. For quantitative analysis the experimental H_2 consumption was compared to that of a known weight of CuO (99.999%) standard.

2.3 Catalytic activity

Catalytic tests were performed in a continuous stainless steel (SS) tubular fixed-bed reactor (ID 7 mm) packed with 0.5 g of catalyst sample. Methanol vapor was introduced into the reactor by a stream of CO_2/He flowing through a SS bubbler containing the liquid alcohol. All reactions were carried out for 3 h at 90°C, 13 bar and total gas flow was about 50 mL min^{-1} (actual flow rate at reaction conditions). Products were monitored online by a mass spectrometer QMS Thermostar 200 (Pfeiffer) with a resolution of 0.01 ppm. Catalytic activity was calculated by methanol conversion (Equation 3), turn over frequency (TOF) (Equation 4) that requires active sites calculation (Equation 5), selectivity (Equation 6) and yield (Equation 7).

$$\text{Methanol conversion} = \frac{[CH_3OH]in - [CH_3OH]out}{[CH_3OH]in} \times 100 \quad (3)$$

$$TOF\left(h^{-1}\right) = \frac{\text{mol } DMC}{h * \#\text{ active sites } (mol)} \quad (4)$$

$$\text{Active sites} = \frac{\text{metal dispersion } (\%)}{100} \times \text{(mol content Cu+mol content Ni)} \quad (5)$$

$$\text{Selectivity } (\%) = \frac{[DMC]}{[DMC] + [by - products]} \times 100 \quad (6)$$

$$\text{DMC yield} = \text{conversion} \times \text{selectivity} \times 100 \quad (7)$$

2.4 Kinetic measurements

The gas-phase experiments were conducted in a stainless-steel fixed bed reactor (ID 7 mm, length of 25 cm) packed with 1 g of catalyst Cu-Ni:2-1, at 12 bar and 110 °C, with different initial CO_2 (0.55-1.65 bar) and methanol partial pressures (0.21-0.83 bar). A CO_2/He mixture was flown through a bubbler filled up with methanol at a given temperature. CO_2, methanol and DMC concentrations (in ppm) were measured online with a mass spectrometer QMS Thermostar 200 (Pfeiffer) equipped with a Secondary Electron Multiplier detector with resolution of 0.01 ppm. The experimental molar fractions of reactants and products were calculated from their partial pressure and the total pressure.

2.5 Kinect modeling

A genetic algorithm (GA) was implemented for parameter fitting; the calculation routine was developed using MATLAB R2008b. Minimization of the difference between the calculated DMC mass fraction y_{calc} and the experimental DMC mass fraction y_{exp} was the objective function for the GA. The optimal solution was the vector of variables that minimized the objective function (Equation 8), defined as the sum of the absolute value of relative deviation between the experimental molar fraction ($y_{exp,i}$) and that calculated from the kinetic equation (y_{calc},i, Equation 9); n is the number of experiments ($n = 11$) [32]. Experimental data for this evaluation are given in Table 2.

$$Fobj = \sum_{i=1}^{n} \left| \frac{y_{exp,i} - y_{calc.i}}{y_{exp.i}} \right| \quad (8)$$

y_{calc} was calculated as

$$y_{cal} = \frac{2r}{v} \times \frac{RT}{P} \quad (9)$$

Where: P = total pressure, R = universal gas constant (0.0082 atm L mol^{-1} K^{-1}), T = temperature [K], v = volumetric flow rate [L s^{-1}], r = reaction rate [mol s^{-1}]. The expression for the reaction rate was obtained from the proposed kinetic mechanism and is shown below in section 3.2.

Table 2 Experimental data for the direct synthesis of DMC

Entry	ppm metanol	ppm CO_2	ppm DMC	y_{DMC}*
1	25183	35007	2,0500	2,0500E-06
2	25344	35585	2,0800	2,0800E-06
3	26133	12684	1,3913	1,3913E-06
4	25528	39340	1,426	1,4260E-06
5	28099	53579,6	1,129	1,1290E-06
6	25807	45056,5	1,323	1,3230E-06
7	30916	20535,01	2,01	2,0100E-06
8	40052,6	34548	3,84	3,8400E-06
9	61188,54	36068	7,27	7,2700E-06
10	10787,41	34258,9	1,79	1,7900E-06
11	34666,2	40117,9	2,63	2,6300E-06

The parameters to be estimated with GA were the kinetic parameters for the proposed model, i.e., the rate constant and the adsorption equilibrium constants for the

species adsorbed on the catalyst surface. For variable optimization, the dependence of the rate constant on temperature was expressed in the form of Arrhenius equation (Equation 10) and that of the adsorption constants as Van't Hoff's equation (Equation 11). Thence, the target variables of the GA were the pre-exponential factor (A) and activation energy (E_a) for the rate constant, and the Gibbs free energies ($\triangle G_i$) for the equilibrium constants. Once the target variables were found by the GA, the rate and adsorption equilibrium constants were directly calculated, and with these the reaction rate and thus y_{calc} were obtained to evaluate the objective function.

$$k = Aexp\left(-\frac{E_a}{RT}\right) \tag{10}$$

$$Keq = exp\left(-\frac{\triangle G}{RT}\right) \tag{11}$$

GA is an optimization method based on natural selection in which a random group of individual solutions is created and then repeatedly modified so that the population evolves until finding an optimal solution [33]. A major advantage of GA is that it can be used in optimization problems that are usually not suitable for standard optimization methods, such as discontinuous, non-differentiable, stochastic or highly non-linear objective functions [33]. Besides, GA explores a large portion of the response surface, is resistant to local optima and bad-conditioned response surfaces, allows determining a number of parameters simultaneously, and does not depend on initial values [34]. Furthermore, GA has been successfully applied for kinetic parameter estimation [34–36].

A roulette-wheel selection function, scattered crossover and gaussian mutation were used, and the distance between individuals of a population and the best and mean individuals was plotted to observe diversity and convergence [33]. Due to the number of variables and their (possible) wide span, a population size of 500 individuals was chosen and a maximum of 100 generations was established. In addition, the GA was run 15 times for every trial to have statistically significant values. Finally, a real coded GA (instead of binary coded) was used as its parameters allow setting wide domains, which increases the precision of the results [35].

2.6 In situ FTIR measurements

In situ infrared spectroscopy measurements were carried out inside a low dead-volume stainless steel transmittance cell equipped with flow and temperature controls (Bruker FTIR spectroscope Tensor series 27, equipped with a TE-DLaTGS detector with stabilized temperature). The cell was capped at both ends (entrance and exit of IR beam) by IR-transparent KBr windows. Powdered monometallic Cu/AC, Ni/AC and bimetallic Cu:Ni-2:1 catalysts were pressed into thin disks with a diameter of 2 cm (10 to 20 mg in weight); each thin disk was then placed inside the cell operating at atmospheric pressure. Due to the opaque nature of carbon-supported metal catalysts the powders for the FTIR studies were dispersed in a commercial Al_2O_3 matrix (99.97% Alfa-Aesar, $<$ 150 mesh) prior to the formation of the disk; alumina was selected because it has been reported as being inert in the direct synthesis of DMC [36], and the signals for methanol and CO_2 on the bare alumina disk were substracted from the spectra of the different samples. Tests were carried out for the adsorption of methanol and CO_2 by flowing a stream of 200 mL min^{-1} of 10 % methanol/N_2 and 5 % CO_2/N_2, respectively. Between 24 and 64 scans in the 4000 to 800 cm^{-1} spectral range, with a scan speed of 2.2 kHz and a resolution of 4 cm^{-1}, were recorded for each spectrum. The spacing of data points was 1.929 cm^{-1}. Before each run (e.g., adsorption of methanol or methanol-CO_2 adsorption), the reactor cell was purged by flowing N_2 for 1 h. The spectra were recorded in Kubelka-Munk units.q

3. Results and discussion

3.1 Catalytic activity

Figure 1 shows the catalytic activity of monometallic and bimetallic samples in terms of MeOH conversion and DMC yield (a), and TOF number (b); no conversion was observed in the bare support.

Bimetallic catalysts display higher conversion and DMC yield than the monometallic ones. Since conversions in the monometallic catalysts were too low, the presence of the second metal is needed to achieve significant activity. Moreover, both conversion and yield follow similar trends with two peaks of activity, for the catalysts with Cu:Ni ratios of 2-1 and 1-3. The best catalytic activity is achieved for an intermediate content of Cu, i.e., for the 2-1 ratio. TOF values, Figure 1 (b), are a better indicator of catalyst activity since they account for the number of active sites of Cu and Ni present in each sample. Similarly to the trend of methanol conversion and DMC yield, Cu/AC or Ni/AC monometallic catalyst displayed very low TOFs. Furthermore, TOF values are much larger in bimetallic catalysts, implying that the synergistic effect of Cu and Ni likely plays a significant role. Catalyst Cu:Ni with a molar ratio of 2:1 showed the highest TOF (73.8 h^{-1}), conversion (2.71%) and yield (2.11%). Selectivity to DMC was above 80%; the main by-products were dimethyl ether (from activation species of methanol) and carbon monoxide (from the cleavage of C–O bond of carbon dioxide), in agreement with [21].

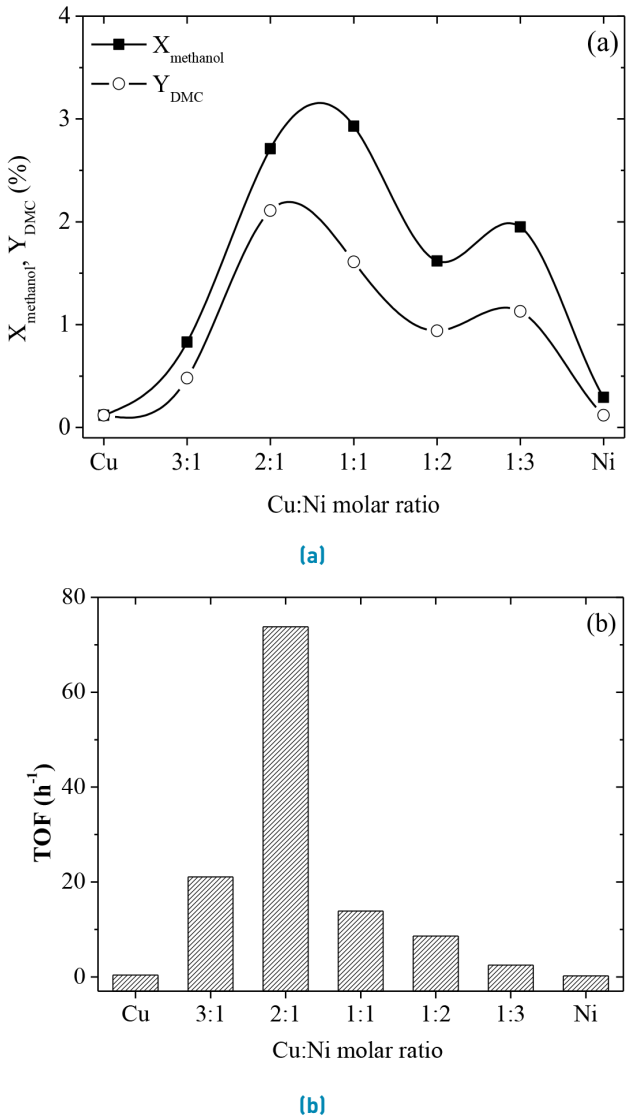

Figure 1 (a) MeOH conversion and DMC yield, (b) TOF values for mono and bimetallic Cu-Ni catalysts tested in the direct synthesis of DMC. 0.5 g of catalyst, 190 psi, 3 h, 90°C; total flow: 50 mL min^{-1}

3.2 Catalyst characterization

XRD and cell parameter of monometallic and bimetallic samples are shown in Figure 2. Activated carbon (not shown) support exhibited a broad and low intensity peak at 2θ = 23°, associated with particular diffraction of activated carbon [21]. The monometallic Cu/AC and Ni/AC samples present a diffraction pattern corresponding to the metallic Ni or Cu face-centered cubic cell with the most intensive diffractions located at 2θ = 43.3° (111) and 50.4° (200) for Cu^0 (JCPDS 4-0836), and 2θ = 44.5° (111) and 51.8° (200) for Ni^0 (JCPDS 4-0850). XRD of Cu-Ni:2-1 bimetallic sample shows characteristic and well defined diffraction peaks related to a cubic phase Cu-Ni alloy at 2θ = 43.7° (111) and 2θ = 50.9° (200), JCPDS 47-1406.

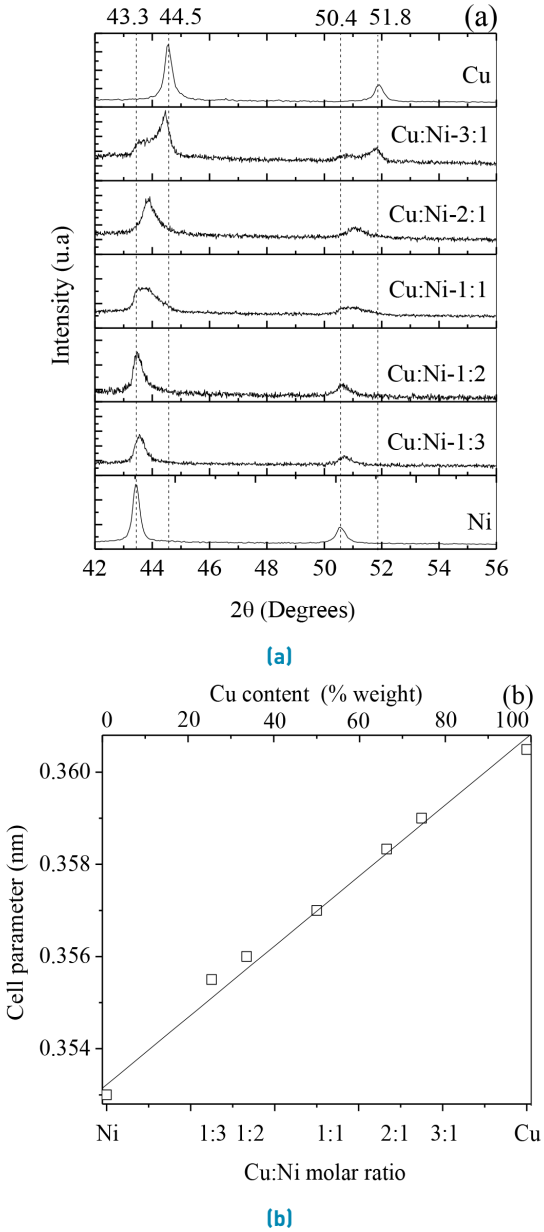

Figure 2 (a) XRD of Cu, Ni and Cu:Ni bimetallic samples and (b) cell parameter of tested catalysts [37]

Indeed, for the bimetallic samples, the diffraction lines corresponding to (111) and (200) Miller indices shift linearly with Cu loading. The increase in the lattice parameter as a function of the Cu concentration, Figure 2b, follows Vegard's Law, i.e., the linear relationship between the lattice parameter of an alloy and the concentration of the two components is an indication of the formation of a Cu-Ni solid solution in the composition range studied [38]. The presence of a Cu-Ni alloy may account for the increased catalytic activity for DMC formation observed with the Cu:Ni molar ratio.

The crystallite size of the copper, nickel and Cu:Ni-2:1 is presented in Table 3. The bimetallic Cu:Ni-2:1 sample presented smaller particle size than the monometallic systems. It is well known that on (relatively) small particles, the fraction of defect sites, e.g., corner sites and low coordination atomic sites, is higher than for relatively large particles, and thus smaller particles exhibit higher number of adsorption sites and higher catalytic activity. In any case, the bimetallic systems are composed for smaller and well dispersed metallic particles contributing to the better DMC behavior.

Table 3 Crystallite size and lattice parameter of Cu, Ni and Cu:Ni-2:1

Sample	θ_B (°)	Crystallite size (nm)
Cu	43.25	23.5
Ni	44.63	17.3
Cu:Ni-2:1	43.57	13.7

Figure 3 presents the TEM images of Cu:Ni-2:1 catalyst with the corresponding particle-size distribution (distributions were fitted with Pearson VII function). The TEM image shows some differences in the morphological characteristics of metal particles. Most particles adopt spherical shape but some particles with rectangular, elliptical and irregular shapes are also observed in both monometallic and bimetallic samples. Generally, metal particles are uniformly dispersed over carbon surface for monometallic samples, whereas particle agglomeration could be observed with Cu-Ni catalyst.

An area survey allowed to extract a particle-size distribution, showing that individual particles consisted of small nanocrystals with an average diameter of 14.33 nm for Cu, Cu-Ni alloy particles, in agreement with XRD results. The mean diameter obtained for Cu-Ni alloy is close to a simple addition between diameters of individual Cu and Ni particles, indicating a possible incorporation of Ni into Cu structure or proximity between particles.

Table 4 summarizes the surface area, metal dispersion, and metal composition of fresh catalyst samples. The BET surface area of all supported catalysts is lower than the surface area of activated carbon (764 m^2 g^{-1}). The reduction of AC surface area, between 10 and 19%, may be associated with the high temperatures at which the samples were subjected to during calcination and activation with hydrogen: 500°C and 600°C, respectively.

Results of metal dispersion may help explain the Cu-Ni interactions in the catalysts. With the exception of catalysts with Cu:Ni molar ratio of 3:1 and 2:1, metal dispersion of all samples was equal to or larger than the monometallic catalysts. The lower dispersion in 3:1 and 2:1 samples is in agreement with the formation of a Cu–Ni

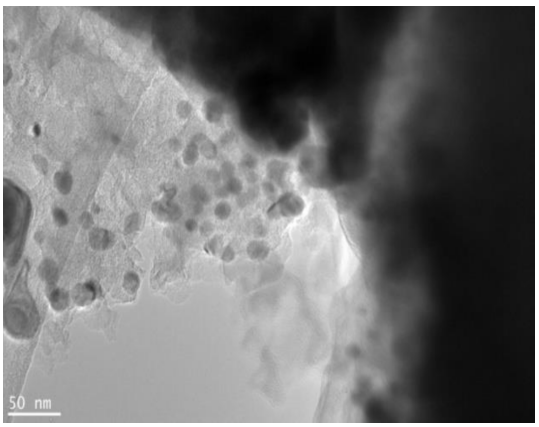

(a)

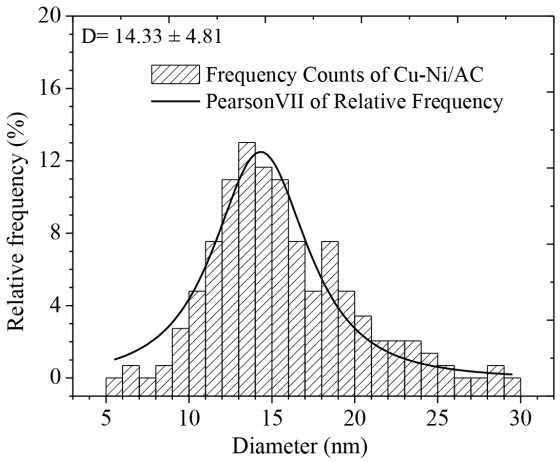

(b)

Figure 3 TEM images (a) and particle size distribution (b) of Cu:Ni-2:1

alloy (which implies a lower presence of species of Cu and Ni metal in an individual manner) with the corresponding "loss" of binding sites for CO (the probe molecule) to chemisorb [39]. Thence, the Cu–Ni interaction, with the possible synergistic effect in activating reactants, increases in the sample with lower dispersion (i.e., higher degree of alloying). Metal dispersion also appears to be related to Ni loading, higher dispersions observed as the nickel loading increased. The reducibility of samples calculated as the ratio of the theoretical and experimental H_2 consumption, indicate that the Cu:Ni-2:1 sample has a higher reducibility percentage (14.9%) than monometallic Cu (11.6%) and Ni (12.7%).

As for the active sites, in the bimetallic Cu:Ni-2:1 catalyst, besides the existence of the Cu-Ni alloy (confirmed by XRD) the presence of water could induce partial oxidation of both metals, being Cu and Ni rapidly oxidized, but the latter presents lower rate of reduction. Therefore, a Cu^0/NiO_x interface may be present in the catalyst. The electronic interchange between those phases could

Table 4 Surface area, metal dispersion and metal loading

Sample	Cu	3:1	2:1	1:1	1:2	1:3	Ni
SA (m^2 g^{-1})	523	670	692	656	617	686	627
Metal Dispersion (%)	0.1	0.02	0.04	0.13	0.25	0.55	0.1
wt. %Cu	12.90	11.03	8.66	7.17	4.45	3.59	-
wt. %Ni	-	2.70	2.79	4.68	5.57	7.68	9.43

provide an electron rich interface where the reactant molecules can be activated and the reaction favored [40].

3.3 FTIR experiments

Based on our FTIR results (shown elsewhere [41]), the main steps in the adsorption of methanol and carbon dioxide on the catalyst surface can be outlined as follows. Methanol is activated by dissociative adsorption to yield a methoxide group and a proton adsorbed on adjacent active metal sites. Carbon dioxide activation forms monodentate carboxylate species, a step that favors the reaction with the oxygen and carbon atoms of the methoxide groups previously formed. Both surface moieties react to form monodentate methyl carbonate species, which is the main intermediate in the production of DMC. In a final reaction step, DMC is formed by reaction between monodentate methyl carbonate groups with methanol from the gas phase, in a step that transfers a methyl group to the surface methyl carbonate and leaves an activated hydroxyl group on the catalyst surface. Water is produced by the reaction between hydroxyl groups and protons adsorbed on metal sites during methanol activation. As the products (dimethyl carbonate and water) desorb from the active sites, these become available for the next catalytic cycle. A hexagonal structure surface model composed of alternate sites with M=O and Mn^{+} vertices was previously postulated [42]. That structure does not match the number of adjacent active sites necessary for the individual reaction steps on the bimetallic Cu-Ni/AC catalyst reported here. Instead, our results are consistent with a tetragonal structure. That structure may also represent the surface of a face-centered cubic structure, in agreement with the XRD characterization, with the center and vertices occupied by active metals M corresponding to either Cu or Ni in the Cu-Ni system.

3.4 Kinetic modeling

The Weisz-Prater (WP) criterion (Equation 12) was used to ensure the absence of diffusion limitations. If WP ≤ 1, limitation in internal mass transfer is negligibly, low.

$$\frac{rR_p^2}{C_o D_{eff}} \leq 1 \tag{12}$$

Where r is the reaction rate and R_p is the particle radius. The effective diffusivity, D_{eff}, was calculated from the molecular diffusion coefficient D_i, porosity ϵ, tortuosity τ and σ is the constriction factor as described in Equation 13.

$$D_{eff} = D_i \times \frac{\in x\sigma}{\tau} \tag{13}$$

Bulk density was calculated as a ratio between mass and volume of the catalyst; both porosity and tortuosity were assumed as 0.4 [43], while the constriction factor value was taken from literature [44], Table 5. The Weisz and Prater criterion calculated at the highest observed reaction rate was 0.15, that is, below the limit of 1.

Table 5 Properties used for evaluating diffusion limitations

Properties	Symbol (units)	Value	Reference
Bed porosity	ϵ	0.4	[43]
Bulk density	ρ_b (g cm^{-3})	0.9	This work
Tortuosity	ρ	0.4	[43]
Constriction factor	σ	0.8	[44]

The proposed reaction mechanism is represented in Figure 4. A non-competitive adsorption is assumed, i.e., methanol and carbon dioxide would interact with different types of active sites $*_A$ and $*_B$ (where $*_A$ and $*_B$ could be Cu, Ni, or Cu-Ni alloy). Dissociative adsorption of methanol, which would provide the bidentate methoxy, methoxide, and hydroxyl groups is represented by Equations 14, 15 and 16, these results are in agreement with [45] who provided experimental FTIR evidence for participation of methoxi and methoxide intermediates in the thermal decomposition of methanol. The adsorption of CO_2 as mono/bidentate carboxylate is depicted by (Equation 17), which has been reported as a typical bonding of carbon dioxide at a transition metal center [46]. Reaction of the carboxylate and methoxy species to produce monodentate methyl carbonate is given by Equation 18. Then, reaction of methoxide species and monodentate methyl carbonate yields dimethyl carbonate and releases two "type A" active sites and one "type B" active site, Equation 19. Finally, water is obtained by reaction of adsorbed hydroxyl and hydrogen groups, Equation 20.

$$CH_3OH + *A \overset{K1}{\leftrightarrow} CH_3OH*A \tag{14}$$

$$CH_3OH + 2*A \overset{K2}{\leftrightarrow} CH_3O*A + H*A \tag{15}$$

$$CH_3OH * A + *A \overset{K3}{\leftrightarrow} CH_3 * A + OH * A \quad (16)$$

$$CO_2 + *B \overset{K4}{\leftrightarrow} CO_2 * B \quad (17)$$

$$CH_3O * A + CO_2 * B \overset{K5}{\leftrightarrow} *ACH_3 * OC(O)O * B \quad (18)$$

$$CH_3 * A + *ACH_3 * OC(O)O * B \overset{K6}{\leftrightarrow} CH_3OC(O)OCH_3 + 2 * A + *B \quad (19)$$

$$OH * A + H * A \overset{K7}{\leftrightarrow} H_2O + 2 * A \quad (20)$$

Reaction of adsorbed carbon dioxide with methoxy species, Equation 18, was chosen as rate determining step due to the slow activation of carbon dioxide [25, 47].

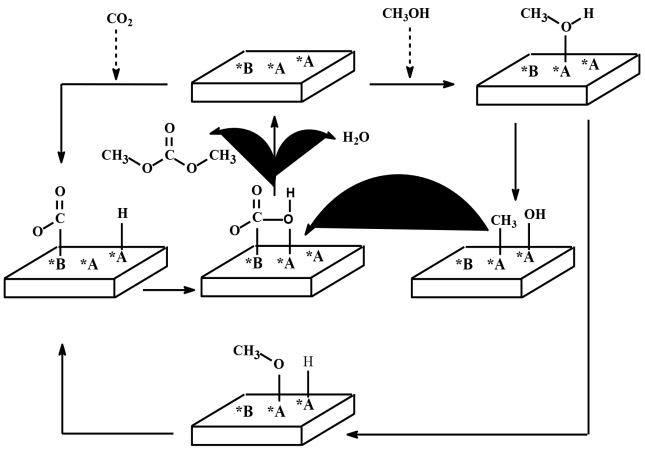

Figure 4 Reaction mechanism of dimethyl carbonate formation from carbon dioxide and methanol over Cu-Ni:2-1/AC catalyst

The rate equation was derived assuming QSSA (quasi steady-state approximation) for each elementary step. Equation 21 shows the obtained kinetic expression.

$$r = k_5 K_1 K_2 K_4 P_{CH3OH} P_{CO2} \theta_A \theta_B (1 - \beta) \quad (21)$$

Where:

$$\beta = \frac{1}{K_1^2 K_2 K_3 K_4 K_5 K_6 K_7} \times \frac{P_{DMC} P_{H2O}}{P_{CH3OH}^2 P_{CO2}} \quad (22)$$

$$\theta_A = \frac{1}{\left(1 + K_1 P_{CH3OH} + K_1 K_2 P_{CH3OH} + \frac{K_1 K_3 K_7 P_{CH3OH}}{P_{H2O}}\right)} + \frac{1}{\left(\frac{P_2}{k_7} + \frac{P_{DMC} P_{H2O} \theta_B}{K_1 K_3 K_6 K_7 P_{CH3OH}}\right)} \quad (23)$$

$$\theta_B = \frac{1}{1 + K_4 P_{CO2} + \frac{P_{DMC} P_{H2O} \theta_A}{K_1 K_3 K_6 K_7 P_{CH3OH}}} \quad (24)$$

β (Equation 22) is defined as the approach-to-equilibrium factor [34], to account for the change in the overall reaction rate in the proximity of the chemical equilibrium; and, θ_A (Equation 23) and θ_B (Equation 24) are the fractions of empty sites. Figure 5 and 6 show the performance of the model and Table 6 presents the kinetic estimated parameters. It can be seen that the kinetic model obtained from the reaction mechanism developed in this work predicts adequately the experimental results; moreover, the model captures both the qualitative and quantitative behavior of the direct synthesis of dimethyl carbonate from CO_2 and methanol over Cu-Ni/AC catalyst.

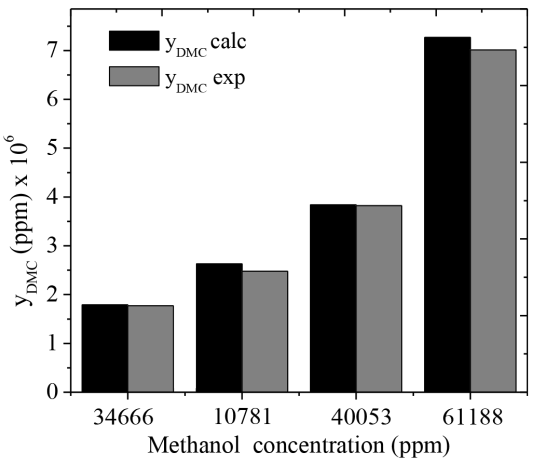

Figure 5 DMC molar fraction, experimental (y_{DMC} exp) and calculated (y_{DMC} calc) from kinetic model, as function of inlet methanol concentration. Reaction conditions: 110 °C, 12 bar, P_{CO2} = 0.27 bar

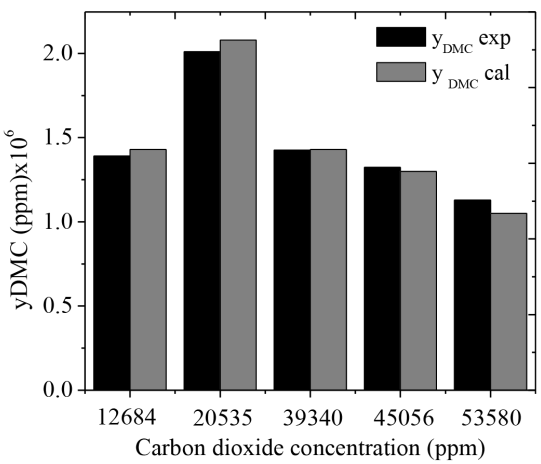

Figure 6 DMC molar fraction, experimental (y_{DMC} exp) and calculated (y_{DMC} calc) from kinetic model, as function of CO_2 inlet concentration. Reaction conditions: 110 °C, 12 bar, P_{CH3OH} = 0.55 bar

Experimental results may help to clarify the proposed

Table 6 Kinetic and equilibrium constants estimated at 110°C for the kinetic of the direct synthesis of DMC from CO_2 and methanol, Equations 11 – 14

Parameter	Description	Value
E_a	Activation energy (J/mol^{-1})	9.424×10^{4}
k_5	Rate constant	6.59×10^{-3}
K_1	Methanol equilibrium adsorption constant	5.81×10^{2}
K_2	Equilibrium constant of methanol dissociation by methoxy group	1.02×10^{2}
K_3	Equilibrium constant of methyl group formation	1.12×10^{-2}
K_4	Carbon dioxide adsorption constant	5.70×10^{1}
K_5	Methyl carbonate group formation from methoxy group and adsorbed carbon dioxide	3.55×10^{18}
K_6	Equilibrium constant of dimethyl carbonate formation from methyl carbonate and methyl species	6.04×10^{-22}
K_7	Equilibrium constant of water formation from OH and H species	4.37×10^{4}
F_{obj}	Given by Equation 1	3.58×10^{-1}

reaction mechanism of the direct synthesis of dimethyl carbonate from carbon dioxide and methanol, Figure 7. Specifically, a Langmuir–Hinshelwood mechanism that includes carbon dioxide and methanol binding to the catalyst in separate steps, as it was suggested in kinetics studies of the liquid phase DMC formation [30], is consistent with the experimental results. The large K_5 value suggests the irreversibility of the surface reaction. The estimated apparent activation energy was 94.2 kJ mol^{-1}.

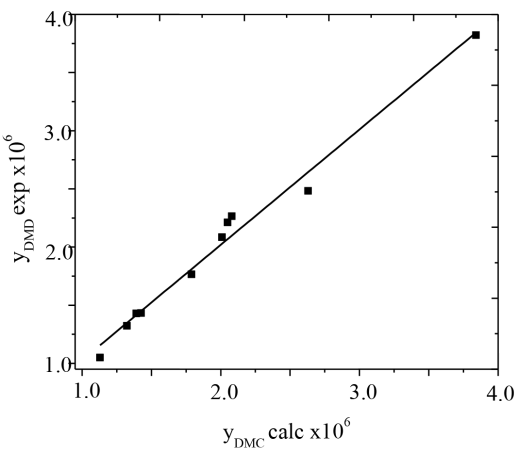

Figure 7 Comparison of calculated and experimental values for dimethyl carbonate formation

The parity plot presented in Figure 7 shows no systematic deviations between the experimental and calculated dimethyl carbonate concentrations. Accuracy of model predictions supports the proposed mechanism as a good representation of the reaction steps.

4. Conclusions

Monometallic Cu and Ni and bimetallic catalysts supported on activated carbon were synthesized and tested for the gas phase formation of DMC from methanol and CO_2. It was found that the catalytic activity of bimetallic samples was higher than monometallic samples. The most active catalyst was the Cu:Ni-2:1 molar ratio sample. The presence of Cu-Ni alloy was evidenced by X-ray diffraction. A kinetic equation was developed for the reaction over Cu-Ni:2-1/AC catalyst. The proposed mechanism was consistent with a Langmuir-Hinshelwood type mechanism where carbon dioxide and methanol are adsorbed on different active sites of the catalyst (Cu, Ni or Cu-Ni solid solution) in two separate steps with the reaction between adsorbed species as rate controlling step. The rate law obtained from the proposed reaction mechanism is in agreement with experimental data. The estimated activation energy was 94.2 kJ mol^{-1}, which is lower than values reported over ceria-based catalysts.

5. Acknowledgments

The authors acknowledge to Universidad de Antioquia for financial support of this work. O.A. acknowledges Universidad Cooperativa de Colombia by grant INV2219.

References

[1] A. Kumar, S. Krishnakumar, and B. Rajasekhar, "Experimental and computational VUV photoabsorption study of dimethyl carbonate: A green solvent," *J. Quant. Spectrosc. Radiat. Transf.*, vol. 217, September 2018. [Online]. Available: https://doi.org/10.1016/j.jqsrt.2018.05.039

[2] J. P. Parrish, R. N. Salvatore, and K. W. Jung, "Perspectives on alkyl carbonates in organic synthesis," *Tetrahedron.*, vol. 56, no. 42, pp. 8207–8237, 2000.

[3] Y. Ono, "Catalysis in the production and reactions of dimethyl carbonate, an environmentally benign building block," *Appl Catal A Gen.*, vol. 155, no. 2, July 31 1997. [Online]. Available: https://doi.org/10.1016/S0926-860X(96)00402-4

[4] Y. Yuan, W. Cao, and W. Weng, "$CuCl_2$ immobilized on amino-functionalized MCM-41 and MCM-48 and their catalytic performance toward the vapor-phase oxy-carbonylation of methanol

to dimethyl carbonate," *J Catal.*, vol. 288, no. 2, December 10 2004. [Online]. Available: https://doi.org/10.1016/j.jcat.2004.09.003

[5] R. Naejus, R. Coudert, P. Willmann, and D. Lemordant, "Ion solvation in carbonate-based lithium battery electrolyte solutions," *Electrochim. Acta*, vol. 43, no. 3-4, 1998. [Online]. Available: https://doi.org/10.1016/S0013-4686(97)00073-X

[6] D. Li, W. Fang, Y. Xing, and R. Lin, "Effects of dimethyl or diethyl carbonate as an additive volatility and flash point of an aviation fuel," *J Hazard Mater.*, vol. 161, no. 2-3, January 30 2009. [Online]. Available: https://doi.org/10.1016/j.jhazmat.2008.04.070

[7] H. Tan and *et al.*, "Review on the synthesis of dimethyl carbonate," *Catal Today.*, vol. 316, October 15 2018. [Online]. Available: https://doi.org/10.1016/j.cattod.2018.02.021

[8] Z. Hou and *et al.*, "High-yield synthesis of dimethyl carbonate from the direct alcoholysis of urea in supercritical methanol," *Chem. Eng. J.*, vol. 236, January 15 2014. [Online]. Available: https://doi.org/10.1016/j.cej.2013.09.024

[9] G. Zhang and *et al.*, "Effect of carbon support on the catalytic performance of Cu-based nanoparticles for oxidative carbonylation of methanol," *Appl. Surf. Sci.*, vol. 455, October 15 2018. [Online]. Available: https://doi.org/10.1016/j.apsusc.2018.05.114

[10] A. H. Tamboli, A. A. Chaugule, and H. Kim, "Catalytic developments in the direct dimethyl carbonate synthesis from carbon dioxide and methanol," *Chem. Eng. J.*, vol. 323, September 1 2017. [Online]. Available: https://doi.org/10.1016/j.cej.2017.04.112

[11] R. Guo and *et al.*, "Enhancement of the catalytic performance in Pd-Cu/NaY catalyst for carbonylation of methyl nitrite to dimethyl carbonate: Effects of copper doping," *Catal. Commun.*, vol. 88, January 5 2017. [Online]. Available: https://doi.org/10.1016/j.catcom.2016.10.007

[12] S. Fujita, B. M. Bhanage, M. Arai, and Y. Ikushima, "Synthesis of dimethyl carbonate from carbon dioxide and methanol in the presence of methyl iodide and base catalysts under mild conditions: effect of reaction conditions and reaction mechanism," *Green. Chem.*, vol. 3, no. 2, April 2014. [Online]. Available: https://doi.org/10.1039/b100363l

[13] B. Fan, H. Li, W. Fan, J. Zhang, and R. Li, "Organotin compounds immobilized on mesoporous silicas as heterogeneous catalysts for direct synthesis of dimethyl carbonate from methanol and carbon dioxide," *Appl. Catal. A Gen.*, vol. 372, no. 1, January 5 2010. [Online]. Available: https://doi.org/10.1016/j.apcata.2009.10.022

[14] K. Tomishige, T. Sakaihori, Y. Ikeda, and K. Fujimoto, "A novel method of direct synthesis of dimethyl carbonate from methanol and carbon dioxide catalyzed by zirconia," *Catal. Lett.*, vol. 58, no. 4, pp. 225–229, May 1999.

[15] K. Tomishige, Y. Furusawa, Y. Ikeda, M. Asadullah, and K. Fujimoto, "CeO_2–ZrO_2 solid solution catalyst for selective synthesis of dimethyl carbonate from methanol and carbon dioxide," *Catal. Lett.*, vol. 76, no. 1-2, pp. 71–74, Sep. 2001.

[16] Y. Yoshida, Y. Arai, S. Kado, K. Kunimori, and K. Tomishige, "Direct synthesis of organic carbonates from the reaction of CO_2 with methanol and ethanol over CeO_2 catalysts," *Catal. Today*, vol. 115, no. 1-4, June 30 2006. [Online]. Available: https://doi.org/10.1016/j.cattod.2006.02.027

[17] M. Aresta and *et al.*, "Influence of Al_2O_3 on the performance of CeO_2 used as catalyst in the direct carboxylation of methanol to dimethylcarbonate and the elucidation of the reaction mechanism," *J. Catal.*, vol. 269, no. 1, January 1 2010. [Online]. Available: https://doi.org/10.1016/j.jcat.2009.10.014

[18] H. Lee, S. Park, I. Song, and J. Jung, "Direct synthesis of dimethyl carbonate from methanol and carbon dioxide over $Ga_2O_3/Ce_{0.6}Zr_{0.4}O_2$ catalysts: Effect of acidity and basicity of the catalysts," *Catal. Letters.*, vol. 141, no. 4, pp. 531–537, Apr. 2011.

[19] S. H. Zhong, J. W. Wang, X. F. Xiao, and H. S. Li, "Dimethyl carbonate synthesis from carbon dioxide and methanol over Ni-Cu/MoSiO (VSiO) catalysts," *Stud. Surf. Sci. Catal.*, vol. 130, 2000. [Online]. Available: https://doi.org/10.1016/S0167-2991(00)80423-1

[20] C. F. Li and S. H. Zhong, "Study on application of membrane reactor in direct synthesis dmc from CO_2 and CH_3OH over Cu–KF/MgSiO catalyst," *Catal. Today*, vol. 82, no. 1-4, July 30 2003. [Online]. Available: https://doi.org/10.1016/S0920-5861(03)00205-0

[21] J. Bian, M. Xiao, S. J. Wang, Y. X. Liu, and Y. Z. Meng, "Highly effective direct synthesis of DMC from CH_3OH and CO_2 using novel Cu–Ni/C bimetallic composite catalysts," *Chinese Chem. Lett.*, vol. 20, no. 3, March 2009. [Online]. Available: https://doi.org/10.1016/j.cclet.2008.11.034

[22] J. Bian and M. Xiao and S. J. Wang and Y. X. Liu and Y. Z. Meng, "Carbon nanotubes supported Cu–Ni bimetallic catalysts and their properties for the direct synthesis of dimethyl carbonate from methanol and carbon dioxide," *Appl. Surf. Sci.*, vol. 255, no. 16, May 30 2009. [Online]. Available: https://doi.org/10.1016/j.apsusc.2009.03.057

[23] J. Bian and *et al.*, "Highly effective synthesis of dimethyl carbonate from methanol and carbon dioxide using a novel copper–nickel/graphite bimetallic nanocomposite catalyst," *Chem. Eng. J.*, vol. 147, no. 2-3, April 15 2009. [Online]. Available: https://doi.org/10.1016/j.cej.2008.11.006

[24] A. Aouissi, A. W. Apblett, Z. AL-Othman, and A. Al-Amro, "Direct synthesis of dimethyl carbonate from methanol and carbon dioxide using heteropolyoxometalates: the effects of cation and addenda atoms," *Transit. Met. Chem.*, vol. 35, no. 8, pp. 927–931, Nov. 2010.

[25] J. Bian and *et al.*, "Direct synthesis of dimethyl carbonate over activated carbon supported Cu-based catalysts," *Chem. Eng. J.*, vol. 165, no. 2, December 1 2010. [Online]. Available: https://doi.org/10.1016/j.cej.2010.10.002

[26] Y. Chen and *et al.*, "Porous diatomite-immobilized Cu–Ni bimetallic nanocatalysts for direct synthesis of dimethyl carbonate," *J. Nanomater.*, vol. 2012, 2012. [Online]. Available: http://dx.doi.org/10.1155/2012/610410

[27] H. Chen and *et al.*, "Direct synthesis of dimethyl carbonate from CO_2 and CH_3OH using 0.4 nm molecular sieve supported Cu-Ni bimetal catalyst," *Chinese J. Chem. Eng.*, vol. 20, no. 5, October 2012. [Online]. Available: https://doi.org/10.1016/S1004-9541(12)60417-0

[28] F. Bustamante, A. Orrego, S. Villegas, and A. Villa, "Modeling of chemical equilibrium and gas phase behavior for the direct synthesis of dimethyl carbonate from CO_2 and methanol," *Ind. Eng. Chem. Res.*, vol. 51, no. 26, May 29 2012. [Online]. Available: https://doi.org/10.1021/ie300017r

[29] B. Santos, C. Pereira, V. Silva, J. Loureiro, and A. Rodrigues, "Kinetic study for the direct synthesis of dimethyl carbonate from methanol and CO_2 over CeO_2 at high pressure conditions," *Appl. Catal. A Gen.*, vol. 455, March 30 2013. [Online]. Available: https://doi.org/10.1016/j.apcata.2013.02.003

[30] C. M. Marin and *et al.*, "Kinetic and mechanistic investigations of the direct synthesis of dimethyl carbonate from carbon dioxide over ceria nanorod catalysts," *J. Catal.*, vol. 340, August 2016. [Online]. Available: https://doi.org/10.1016/j.jcat.2016.06.003

[31] O. Arbeláez, A. Orrego, F. Bustamante, and A. L. Villa, "Direct synthesis of diethyl carbonate from CO_2 and CH_3CH_2OH over Cu–Ni/AC catalyst," *Top. Catal.*, vol. 55, no. 7-10, pp. 668–672, Jul. 2012.

[32] M. Maeder, Y. M. Neuhold, and G. Puxty, "Application of a genetic algorithm: near optimal estimation of the rate and equilibrium constants of complex reaction mechanisms," *Chemom. Intell. Lab. Syst.*, vol. 70, no. 2, February 28 2004. [Online]. Available: https://doi.org/10.1016/j.chemolab.2003.11.006

[33] S. Katare, A. Bhan, J. M. Caruthers, W. N. Delgass, and V. Venkatasubramanian, "A hybrid genetic algorithm for efficient parameter estimation of large kinetic models," *Comput. Chem. Eng.*, vol. 28, no. 12, November 15 2004. [Online]. Available: https://doi.org/10.1016/j.compchemeng.2004.07.002

[34] H. Lynggaard, A. Andreasen, C. Stegelmann, and P. Stoltze, "Analysis of simple kinetic models in heterogeneous catalysis," *Prog. Surf. Sci.*, vol. 77, no. 3-4, November 2004. [Online]. Available: https://doi.org/10.1016/j.progsurf.2004.09.001

[35] C. Jiang and *et al.*, "Synthesis of dimethyl carbonate from methanol and carbon dioxide in the presence of polyoxometalates under mild conditions," *Appl. Catal. A Gen.*, vol. 256, no. 1-2, December 30 2003. [Online]. Available: https://doi.org/10.1016/S0926-860X(03)00400-9

[36] J. M. Nougués, M. D. Grau, and L. Puigjaner, "Parameter estimation

with genetic algorithm in control of fed-batch reactors," *Chem. Eng. Process. Process. Intensif.*, vol. 41, no. 4, April 2002. [Online]. Available: https://doi.org/10.1016/S0255-2701(01)00146-5

[37] S. D. Harris, L. Elliott, D. B. Ingham, M. Pourkashanian, and C. W. Wilson, "The optimisation of reaction rate parameters for chemical kinetic modelling of combustion using genetic algorithms," *Comput. Methods. Appl. Mech. Eng.*, vol. 190, no. 8-10, November 24 2000. [Online]. Available: https://doi.org/10.1016/S0045-7825(99)00466-1

[38] K. Tomishige, Y. Ikeda, T. Sakaihori, and K. Fujimoto, "Catalytic properties and structure of zirconia catalysts for direct synthesis of dimethyl carbonate from methanol and carbon dioxide," *J. Catal.*, vol. 192, no. 2, June 10 2000. [Online]. Available: https://doi.org/10.1006/jcat.2000.2854

[39] A. F. Orrego and F. Bustamante, "Direct synthesis of dimethyl carbonate from CO_2 and methanol in gas-phase," M.S. thesis, Dept. Chem. Eng., Universidad de Antioquia, Medellin, Colombia, 2014.

[40] S. A. Khromova and *et al.*, "Anisole hydrodeoxygenation over Ni–Cu bimetallic catalysts: The effect of Ni/Cu ratio on selectivity," *Appl. Catal. A Gen.*, vol. 470, January 30 2014. [Online]. Available: https://doi.org/10.1016/j.apcata.2013.10.046

[41] O. Arbelaez and *et al.*, "Conversion of carbon dioxide and methanol into dimethyl carbonate using Cu-Ni supported on activated carbon. theoretical and in situ FTIR studies," unpublished.

[42] S. H. Zhong, J. W. Wang, X. F. Xiao, and H. S. Li, "Dimethyl carbonate synthesis from carbon dioxide and methanol over Ni-Cu/MoSiO(VSiO) catalysts," *Stud. Surf. Sci. Catal.*, vol. 130, 2000. [Online]. Available: https://doi.org/10.1016/S0167-2991(00)80423-1

[43] C. Karakaya, R. Otterstätter, L. Maier, and O. Deutschmann, "Kinetics of the water-gas shift reaction over Rh/Al_2O_3 catalysts," *Appl. Catal. A Gen.*, vol. 470, January 30 2014. [Online]. Available: https://doi.org/10.1016/j.apcata.2013.10.030

[44] G. Carotenuto, R. Tesser, M. D. Serio, and E. Santacesaria, "Kinetic study of ethanol dehydrogenation to ethyl acetate promoted by a copper/copper-chromite based catalyst," *Catal. Today*, vol. 203, March 30 2013. [Online]. Available: https://doi.org/10.1016/j.cattod.2012.02.054

[45] J. Zawadzki, B. Azambre, O. Heintz, A. Krztoń, and J. Weber, "IR study of the adsorption and decomposition of methanol on carbon surfaces and carbon-supported catalysts," *Carbon*, vol. 38, no. 4, 2000. [Online]. Available: https://doi.org/10.1016/S0008-6223(99)00130-X

[46] X. Yin and J. R. Moss, "Recent developments in the activation of carbon dioxide by metal complexes," *Coord Chem Rev.*, vol. 181, no. 1, January 1999. [Online]. Available: https://doi.org/10.1016/S0010-8545(98)00171-4

[47] S. Y. Zhao, S. P. Wang, Y. J. Zhao, and X. B. Ma, "An in situ infrared study of dimethyl carbonate synthesis from carbon dioxide and methanol over well-shaped CeO_2," *Chinese Chem. Lett.*, vol. 28, no. 1, January 2017. [Online]. Available: https://doi.org/10.1016/j.cclet.2016.06.003